Journal of Molecular Science

Journal of Molecular Science
Volume 36 Issue 2, Year of Publication 2026, Page 464-473
DoI-10.004687/1000-9035.2026.056

Journal of Molecular Science
www.jmolecularsci.com ISSN:1000-9035

Investigation of Copolymers: Metal Oxide Ternary Nanocomposites for Sensing Application

R. Murugan[1], Dr. R. Thiyagarajan[2], Dr. S. Vignesh[3] , Dr. S.Tamilselvan[4]

[1]Ph.D Research Scholar, PG & Research Department of Physics, Chikkaiah Naicker College, Erode-638004, Tamilnadu, India.
[2]Associate Professor, PG & Research Department of Physics, Chikkaiah Naicker College, Erode-638004, Tamilnadu, India.
[3]Assistant Professor, Department of Mechanical Engineering, Sree Sakthi Engineering College(Autonomous), Coimbatore-64104, Tamilnadu, India.
[4]Assistant Proessor, Department of Physics, Nandha arts and Science College, Erode-638052, Tamilnadu, India.

Article Information
Received: 17-04-2026
Revised: 13-05-2026
Accepted: 04-06-2026
Published: 27-06-2026

Keywords
electrochemical sensors, SEM, XRD and FT-IR

ABSTRACT
In recent years, the electrochemical sensors are used comprehensively due to their inimitable properties. Conducting polymers are well known their inbuilt charge transfer properties. The morphological and composite properties of PANI/CuO Composites were examined by SEM, XRD and FT-IR. [1] The humidity sensing chattels of the PANI/CuO nanocomposites was inspected by exposing to a broad range of 0-97%RH. The humidity sensing properties of the Modification of conducting polymers using metal oxides enhance the sensitivity, stability and resproductibility of the electrode which enhances the overall sensor performance [2]. The FTIR spectrum exposed a peak at 1462 cm^{-1} corresponding to the N=N stretching in the copolymer structure. The solubility test declared that the primed copolymers are freely soluble in water. The CuO nanoparticles interceded haphazard copolymer revealed an increase in electrical conducting value. A plausible explicate the experimental results obtained. Nanocomposite natural polymer/metal oxide is an attractive new expertise for abundant solicitations as sensors, coatings and electronic devices.

1. INTRODUCTION:

Researchers in science and technology have been engrossed in polymeric materials for their copious uses. In light of its use in electronic and optical devices, research on the polymer's electrical and optical appearances has recently garnered much devotion. Research in the field of electrically conducting copolymers has customary considerable kindness due to its ease of synthesis, processability and tenders in various sciences and engineering fields.[1] The invention of new substances with outstanding properties often leads to latest technology. Because of their extraordinary properties such as electrical characteristics, reversible doping-dedoping procedure, controllable chemical and electrochemical properties and simple processibility, a variety of CPs e.g., polyacetylene (PA), Polyaniline (PANI), polypyrrole. Conducting polymer segment several characteristics; including macro molecular character and electrical transport properties. All the case with poly acetylene is the humblest conducting polymer, in which the electrical transport characteristics are locating by placing the alternate carbon twofold bond structure direction on the back bone of polymer. The polymers themselves are not new; many of them such as polypyrrole are well notorious in their non-conducting form before their conductivity was revealed.

2. Experimental and methods

Aniline, known as phenylamine or aminobenzene, is

an organic compound with the formula $C_6H_5NH_2$. Consisting of a phenyl group involved to an amino group, aniline is an aromatic amine. Among the conducting polymer, Polyaniline (PANI) is one such polymer whose synthesis does not require any superior equipment or precautions. High-tech uses depend significantly on the reproducible control of the molecular and supramolecular architecture of the macromolecular via a unpretentious methodology of organic synthesis. O-Toluidine (C_7H_9N) is a clear colorless or light-yellow liquid. May become reddish brown on exposure to air and light. Poly(O-Toluidine) (POT) is a imitative of PANI, which comprehends the $–CH_3$ group into the ortho position of the aromatic ring of the aniline monomer. Among the ring substituted PANI derivatives, POT has been most widely studied one because of its interesting electro-optical properties.

Reagents (KMnO4, Aniline, Ammonium persulfate (APS), Pyrrole) and solvents (H2SO4, H2O2, HCl, CH3OH) were of analytical grade. The water for all experiments was ultrapure water (≥18.43 MΩ·cm).

5.1. XRD ANALYSIS

X-ray diffraction (XRD) spectra of all the samples recorded by Phillips Expert PW3020 diffractometer using Cu Kα radiation (λ=1.54056 Armstrong) were presented for structural analysis of the samples.

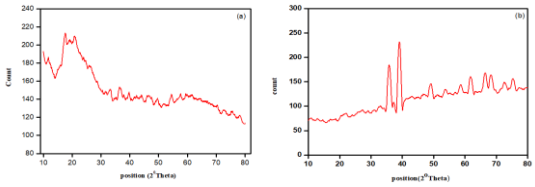

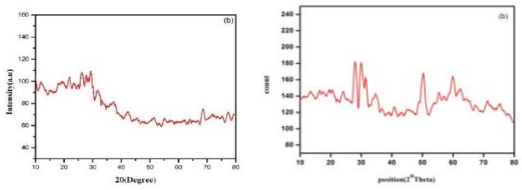

Fig 5.1 XRD pattern of (a)poly(ani;o-tol);MnO_2, (b)poly(ani;o-tol);MnO_2,CuO, (c) Poly(ani-o-toluidine) +MnO_2+ZrO_2 and d) Poly(ani-o-tol);MnO_2+CdO

The XRD pattern of Poly(ani-o-toluidine) +MnO_2+CuO (5.1.a) shows a Sharpe peak at 2θ=35.8°(d=0.25), indicates broad crystalline nature. This characteristic peak of Poly(ani-o-toluidine) +MnO_2+ZrO_2 is ascribed to the periodicity in parallel and perpendicular directions of the polymer. The XRD pattern of copolymers Poly(ani-o-toluidine) +MnO_2+CuO (fig 5.1a) shows a Sharp peak at 2θ=39.04°(d=0.23) crystalline behaviour. The XRD pattern of Poly(ani-o-toluidine) +MnO_2+CuO and Poly(ani-o-toluidine) +MnO_2+ZrO_2 are shown in fig 5.1 (a and b). The characterization peaks ascertained from the XRD pattern of copolymers are at 2θ=26.28° (d=0.34) and 2θ=29.35°(d=0.30) Poly(ani-o-toluidine) +MnO_2+CuO and 2θ=26.28° (d=0.34) and 2θ=29.35°(d=0.30) Poly(ani-o-toluidine) +MnO_2+ZrO_2, broad crystalline diffraction peak due to the presence of benzoid rings of copolymer. The crystalline sizes and dislocation density are calculated and tabulated as shown in Table 5.1. As compared to (a) Poly(ani-o-toluidine) +MnO_2+CuO, (b) Poly(ani-o-toluidine) +MnO_2+ZrO_2, the crystallite sizes increase for the copolymer materials.

Table 5.1 XRD spectrum for (a)Poly(ani-o-toluidine) +MnO_2+CuO, (b) Poly(ani-o-toluidine) +MnO_2+ZrO_2

S.No	Sample name	2θ (deg)	FWHM (deg)	Intensity	d spacing (Å)	Crystal size (nm)	Dislocation density x10^{15}
1	Poly(ani-o-toluidine) +MnO_2+CuO	35.8	1.34649	118.94764	0.25	6.48	0.023814
		39.04	1.24798	165.70312	0.23	7.06	0.020062
2	Poly(ani-o-toluidine) +MnO_2+ZrO_2	26.28	1.04	108.226971	0.34	8.20	0.014872
		29.35	1.2	109.514752	0.30	7.15	0.019560

The X-ray diffraction (XRD) spectra of all samples recored by Phillips expert PW3020 diffractometer using cu ka radiation (wavelength=1.54056) were presented for structural analysis of the samples. The XRD pattern of poly(ani-o-tol) (5.1.a) shows a Sharpe peaks at 2θ=17.3546(d=5.10573), indicates broad crystaline nature. This characteristic peak of poly(ani-o-tol) is ascribed to the periodicity in parallel and perpendicular directions of the polymer. The XRD pattern of Poly(o-tol) (5.2.b) shows a Sharpe peaks at 2θ=75.3138˚ (d=1.26190) crystalline behavior, The XRD pattern of poly(ani-o-tol) (1:2) and Poly(o-tol) (2:1) copolymers are shown in Fig.5.2. The characterization peaks ascertained from the XRD pattern of copolymers are at 2θ = 35.9153^0(d=2.50049) Poly(o-tol) (1:1), 2θ = 39.0971 (d=2.30402) poly(ani-o-tol) (1:2) and 2θ = 49.0500^0 (d=1.85728) poly(ani-o-tol) (2:1) , 2θ = 61.9074 (d=1.49651) 2θ = 66.4763 (d=1.40651) , 2θ =68.4096(d=1.37140), 2θ =72.7468(d=1.29996), 2θ =75.3138(d=1.26190) broad crystal diffraction peak due to the presence of benzoid and quinoid rings of copolymer.

Table 5.1 XRD pattern of (a)poly(ani;o-tol);MnO_2.

Pos[^{0}2Th.]	Height[cts]	FWHM Left[^{0}2th.]	d-spacing[A]	Rel.int.[%]
17.3546	35.50	0.5760	5.1073	100.00

The crystalline sizes and dislocation density are calculated and tabulated as shown in Table 5.1 As compared to poly(ani-o-tol), the crystallite sizes in decreased for the copolymer materials.

Table 5.2 XRD pattern of (b)poly(ani;o-tol);MnO_2,CuO ternary composites

Pos[^{0}2Th.]	Height[cts]	FWHM Left[^{0}2th.]	d-spacing[A]	Rel. int.[%]
35.9153	132.14	0.2755	2.50049	42.94
39.0971	307.75	0.1574	2.30402	100.00
49.0500	50.03	0.4723	1.85728	16.26
61.9074	76.50	0.3149	1.49887	24.86
66.4763	45.06	0.7872	1.40651	14.6
68.4096	51.38	0.5510	1.37140	16.69
72.7468	29.93	0.4723	1.29996	9.73
75.3138	30.92	0.9446	1.26190	10.05

Pos. [°2Th.]	Height [cts]	FWHM Left [°2Th.]	d-spacing [Å]	Rel. Int. [%]
14.2589	5.04	3.7786	6.21164	5.61
28.0443	86.77	0.3149	3.18179	96.59
30.0940	89.83	0.3936	2.96958	100.00
31.3221	49.51	0.4723	2.85589	55.11
35.1235	32.65	0.4723	2.55503	36.35
50.1623	81.38	0.3936	1.81867	90.60
55.5529	19.00	0.9446	1.65429	21.15
59.9758	37.74	0.6298	1.54244	42.01

The X-ray diffraction of acids doped MnO_2-ZrO_2 with APS oxidants are shown in Fig 5.1 respectively. The 2 Theta value are shown in the XRD patterns (Fig 5.1). The X -ray diffraction pattern of (a) poly (ani:o-tol) MnO_2: ZrO_2. has a broad peak at (^{0} 2 Theta) =26.31^0? The some sharp peaks at 27^0,29^0 and 33^0 are simply due to the semi-crystalline structure of Poly (ani:o-tol): MnO_2: ZrO_2. The X-ray diffraction of acids doped MnO_2-CdO with APS oxidants are shown in Fig 5.1 respectively. The 2 Theta value are shown in the XRD patterns (Fig 5.1). The X -ray diffraction pattern of (b) poly (ani:o-tol) MnO_2, CdO has a broad peak at (^{0} 2 Theta) =14^0. The some sharp peaks at 28^0,30^0, 31^0,35^0,50^0,55^{0}and 59^0 are simply due to the semi-crystalline structure of Poly(ani:o-tol): MnO_2: CdO.

Table 5.1 (a) Poly (ani:o-tol): MnO_2:ZrO_2

Pos. [°2Th.]	Height [cts]	FWHM Left [°2Th.]	d-spacing [Å]	Rel. Int. [%]
26.3135	42.18	0.3149	3.38701	68.30
27.7897	30.76	0.4723	3.21036	49.81
29.0024	61.76	0.2362	3.07882	100.00
29.7145	38.16	0.2362	3.00663	61.78
33.8288	20.70	0.2362	2.64979	33.51

FTIR Studies:

The functional group of Poly(ani-o-toluidine) +MnO_2+CuO and Poly(ani-o-toluidine) +MnO_2+ZrO_2 copolymers powders were recorded using KBr pellets. Fig 5.2 shows the FTIR spectrum of Poly(ani-o-toluidine) +MnO_2+CuO and Poly(ani-o-toluidine) +MnO_2+ZrO_2 in the range of 450 cm^{-1} to 4000cm^{-1}. The structural information on all the electrode materials was identified by FTIR spectra. The spectrum of Poly(ani-o-toluidine) +MnO_2+CuO (Fig 5.2 a) acquires the main characteristic peak at 769.01844 cm^{-1}, 876.044879 cm^{-1}, 1284.83759 cm^{-1}, 1596.26039 cm^{-1}, 3037.49611 cm^{-1} and 3392.37325 cm^{-1}. The strong peak in range 3392.37325 cm^{-1} corresponds to N-H band stretching vibration. The peak at 3037.49611 cm^{-1} corresponds to =C-H stretching vibration. The presence of sharp peak at 1596.26039 cm^{-1} and is attributed to C=N and C=C stretching vibration for the quinoid ring. The peak at 1284.83759 cm^{-1} attributed to C-N stretching mode of benzenoid and quinoid rings. The peak at 876.044879 cm^{-1} is associated with C-H stretching for a benzenoid ring.

The spectrum of Poly(ani-o-toluidine) +MnO_2+ZrO_2 (Fig.5.1. b) acquires the main characteristic peaks at 3398.49922, 3006.04199, 2893.91135, 1522.71384, 1290.44323, 1067.78383, 864.346812, 767.433904 cm^{-1}. The strong and broad peak in the range at 3398.49922 cm^{-1} correspond N-H band stretching vibration. The strong peak at 3006.04199 cm^{-1} corresponds to C-H stretching mode. The presence of sharp peak at 2893.91135 cm^{-1} is attributed to C-H aldehydic stretching mode. The presence of sharp peak at 1522.71384 cm^{-1} corresponds to C=O stretching vibration. The peak at 1290.44323 cm^{-1} is attributed to C-N and C=N stretching modes. The peak at 1067.78383 cm^{-1} is attributed to C-N stretching mode of benzenoid and quinoid rings. The peak at 864.346812 cm^{-1} is associated with C-H stretching for a benzenoid ring.

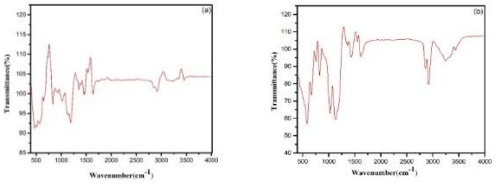

Fig.5.2. FTIR spectrum for (a) Poly(ani-o-toluidine) +MnO_2+CuO, (b) Poly(ani-o-toluidine) +MnO_2+ZrO_2

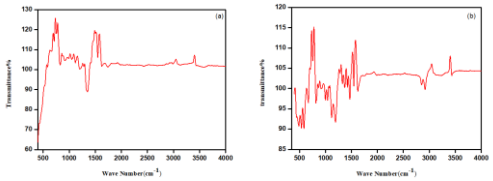

Fig 5.2 FTIR pattern of (a)poly(ani;o-tol);MnO_2 and (b)poly(ani;o-tol);MnO_2,CuO

Table.5.2. FTIR spectrum for (a) Poly(ani-o-toluidine) +MnO_2+CuO, (b) Poly(ani-o-toluidine) +MnO_2+ZrO_2

Characteristic vibration	Wavelength(cm^{-1})	
	Poly(ani-o-toluidine) +MnO_2+CuO	Poly(ani-o-toluidine) +MnO_2+ZrO_2
N−H stretching vibration	3392.37325	3398.49922
=C-H stretching	3037.49611	3006.04199
C=N and C=C stretching vibration	1596.26039	2893.91135
C-N stretching mode	1284.83759	1290.44323
C-H stretching	876.044879	864.346812

The functional group of Copolymers (PANI-Co-POT) powders were recorded using KBr pellets. Fig 5.2a shows the FTIR spectrum of Co-polymers (PANI-Co-POT) in the range of 400 -4000 cm^{-1}. The structural information on all the electrode materials was identified by FTIR spectra. The spectrum of Co-polymers (PANI-Co-POT) + MnO_2 (Fig 5.1a) acquires the main characteristics peaks at 692.664577, 740.815047, 782.194357, 1487.14734 and 1583.44828 cm^{-1}.

The strong broad peak in range 1583.44828 cm^{-1} corresponds to C-N amide II band. The peaks is associated with 1487.14734 is stretching –C=o inorganic carbonate. The peak is associated with 782.194357 cm^{-1} and 740.815047cm^{-1} is bending –C=o inorganic carbonate. The peak is associated with 692.664577 is bending CH out of plane aromatic band. The Fig 5.2 (b) acquires the main characteristics peaks at 735.977011, 782.507837, 1300.44932, 1520.13584, 1579.63427 cm^{-1}. The strong broad peak in range 1579.63427 cm^{-1} is corresponds to C-N amide II band. The peaks is associated with 1520. 13584is stretching C-N amide II band. The peaks is associated with 1300.44932 is stretching C-N amide III band. The peak is associated with 735.944011cm^{-1} and 782.507837 is bending –C=o inorganic carbonate.

Table 5.3 FTIR pattern of (a)poly(ani;o-tol);MnO_2 and (b)poly(ani;o-tol);MnO_2,CuO

Functional group	Standard Vibrational Stretching frequency cm^{-1}	Observed vibrational Stretching frequency cm^{-1}
CH out of plane aromatic band	690 cm^{-1}	692.664577 and 735.977011
CH out of plane aromatic band	690 cm^{-1}	782.507837 and 740.815047
CH out of plane aromatic band	690 cm^{-1}	782.194357
C-N amide III band	1,240-1,340 cm^{-1}	1300.44932
C-N amide II band	1540 cm^{-1}	1487.14734 and 1520.13584
C-N amide II band	1540$^{-1}cm^{-1}$	1583.44828 and 1579.63427

FT-IR spectra of and acid doped MnO_2-ZrO_2 and MnO_2-CdO synthesized with APS oxidant are shown in Fig 5.2. The functional group attached to the aromatic ring have been identified by the presence of absorption peaks. The spectrum of Fig.5.1 (a&b) acquires the main characteristic peaks at 641, 729, 785, 1075, 1303, 1514, 1571, 3003 and 3406 cm^{-1}. The strong broad peak in range 3406 cm^{-1} corresponds to H-O band stretching vibration.

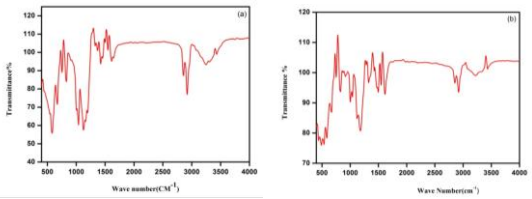

Fig 5.2 FTIR pattern of (a) Poly (ani:o-tol): MnO_2:ZrO_2 and (b) CoPoly (ani:O-Tol): MnO_2, CdO ternary nanocomposites

The MnO_2-ZrO_2 and MnO_2-CdO samples recorded in the range of 400-5000 cm^{-1}. The KBr mode has been used to record the spectra. The FT-IR spectrum shown broad stretching vibrational bands around 641 and 646 cm^{-1} appear typically due to stretching and banding modes of CH group. The strong broad peak in range 3406 cm^{-1} corresponds to H-O band stretching vibration. The presence of sharp peaks at 1075 cm^{-1} are attributed to C-O stretching vibration for the quinoid and benzenoid rings. The peaks at 1303 cm^{-1} and 1313 cm^{-1} are attributed to CH aliphatic banding group stretching mode of benzenoid and stretching modes. The peak at 3003 cm^{-1} is associated with CH stretching alkenes group for a benzenoid ring.

Table 5.3 FTIR Table of (a) Poly (ani:o-tol): MnO_2:ZrO_2 and (b) CoPoly (ani:O-Tol): MnO_2, CdO ternary nanocomposites

Functional group	Standard vibrational stretching frequency Cm^{-1}	Obserced vibrational stretching frequency cm^{-1}
CH	690 cm^{-1}	641 and 646
C-O	1080 CM^{-1}	1075
CH aliphatic	1370 cm^{-1}	1303 and1313

banding group		
Aromatic	1510 cm^{-1}	1514 and1406
C-N amide II Band	1540 cm^{-1}	1571 and1525
CH stretching alkenes group	3010 cm^{-1}	3003 and3054
O-H group	3420 cm^{-1}	3406 and3406

UV Studies:

The electronic properties of the Poly(ani-o-toluidine) +MnO_2+CuO and Poly(ani-o-toluidine) +MnO_2+ZrO_2 UV-visible absorption spectroscopy analyses were performed. Fig 5.3 represents the UV-visible spectra of the Poly(ani-o-toluidine) +MnO_2+CuO and Poly(ani-o-toluidine) +MnO_2+ZrO_2. All the powders are dissolved in DMSO solvent for UV-Visible is spectroscopy analysis.

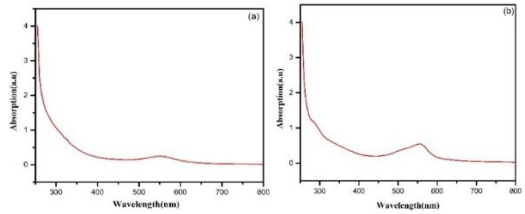

Fig.5.3. UV spectrum for (a) Poly(ani-o-toluidine) +MnO_2+CuO, (b) Poly(ani-o-toluidine) +MnO_2+ZrO_2

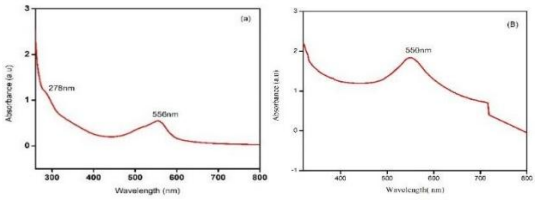

Fig 5.2 UV-Vis absorption spectra of (a) Pani-MnO2-ZrO2 and (b) Pani-MnO2-CdO.

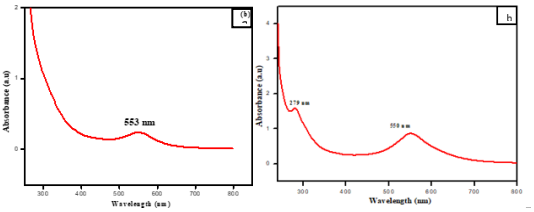

Fig 5.2 UV-Vis absorption spectra of (a) Poly (ani:O-tol) - MnO2 and (b) Poly (ani:O-tol)-MnO2-CuO

It is observed from the Fig 5.3 (a) that Poly(ani-o-toluidine) +MnO_2+CuO has one absorption band at 551 nm. The absorption band 551 nm is assigned to the n-π* transition of benzenoid to quinoidexcitonic transition. Fig 5.3 (b) that Poly(ani-o-toluidine) +MnO_2+ZrO_2 has two characteristics absorption bands at around 284 nm and 553 nm. The absorption peak at 284 nm is assigned to the π-π* transition of the benzene rings. The absorption peak at 553 nm is assigned to the n-π* transition of benzenoid. The optical band gaps of Poly(ani-o-toluidine) +MnO_2+CuO and Poly(ani-o-toluidine) +MnO_2+ZrO_2 Copolymer nanoparticles obtained from Table are 2.25eV, 4.37eV and 2.24eV. This implies that there was a strong interaction between Poly(ani-o-toluidine) +MnO_2+CuO and Poly(ani-o-toluidine) +MnO_2+ZrO_2 nanoparticles are decrease in the bandgap when comparing to Poly(ani-o-toluidine) +MnO_2+CuO and Poly(ani-o-toluidine) +MnO_2+ZrO_2. In UV analysis the bandgap energy of copolymers and their corresponding electron transition are tabulated in Table 5.2.

Table 5.3 UV peaks and their electron transition and bandgap energy of (a)Poly(ani-o-toluidine) +MnO_2+CuO, (b) Poly(ani-o-toluidine) +MnO_2+ZrO_2

S.No	Sample name	Wavelength(nm)	Electron transition	Bandgap energy(eV)
1	Poly(ani-o-toluidine) +MnO_2+CuO	551	n-π*	2.25
2	Poly(ani-o-toluidine) +MnO_2+ZrO_2	284	π-π*	4.37
		553	n-π*	2.24

The UV-Vis absorption spectra for Pani-MnO2-ZrO2 and Pani-MnO2-CdO nanocomposites are recorded at room temperature are given in Fig 5.1. It is observed from the Fig. 5.1 (a) that PANI has two characteristics absorption bands at around 278nm to 556nm represent. The absorption peak at 278nm is assigned . Fig. 5.1 (b) shows peak at 550nm represent. By Comparing to sample 2, sample 1 gets two peaks and sharp peaks. The addition two nanoparticles shows the two sharp peaks.

Fig 5.2 UV-Visible Spectroscopy of (a) Pani-MnO2-ZrO2 and (b) Pani-MnO2-CdO.

SAMPLE	WAVELENGTH	BANDGAP
poly(ani:o-tol) MnO2 + ZrO2	278 & 556	4.46ev and 2.23eV
poly(ani:o-tol) MnO2 +CdO	55O	2.25Ev

The calculated optical bandgap values 4.46ev and 2.23eV respectively. (PANI-MnO2- ZrO2) is territory composites . The UV-Vis absorption spectra for Poly-(ani:O-tol)-MnO2 and Poly-(ani:O-tol)-MnO2-CuO nanocomposites are recorded at room temperature are given in Fig 5.1. All the powders aredissolved in DMSO solvent for UV-Visible is spectroscopy analysis.

Fig. 5.2 (a) shows peak at 553 nm represents Poly (ani:O-tol)- MnO2. Fig. 5.2 (b) shows peak at 279 nm and 550 nm represents Poly (ani:O-tol)-MnO2-CuO. The absorption peak at 279nm and 550nm is assigned to π-π* transition of the benzene rings. The absorption peak at 553nm is assigned to the π-π* transition of the benzene rings. Fig. 5.2 (b) shows that Poly (ani:O-tol)-MnO2-CuO has two

characteristics absorption bands around 279nm and 550nm. It indicates that the insertion of nanoparticles of MnO2 and CuO has an effect on the doped Poly-(ani:O-tol). It indicates that the addition of two nanoparticles has a significant influence in the composite matrix. The addition two nanoparticles shows the two sharp peaks and the polymer ternary composite (B) is used for the morphological studies.

SEM Analysis: (EDAX)

In Fig. 5.5, the SEM morphology of the Poly(ani-o-toluidine)-MnO_2-CuO nanocomposites is depicted. It is observed that the particle shown in Fig 5.5 consists of small grains, with sizes smaller than 1mm, which have agglomerated. These grains exhibit the laminar structure that is characteristic of these materials. A uniform surface with good aggregation, as seen in Fig 5.5, is confirmed for the DBSA doped Poly(ani-o-toluidine)-MnO_2-CuO. At higher magnification, as shown in Fig 5.5, a sponge-like structure with an aggregation of small, uniform-sized granular domains is developed in the prepared Poly(ani-o-toluidine)-MnO2-CuO nanocomposites. The morphology of the nanocomposites, which varies with the addition of nanoparticles, is exhibited in Fig 5.5. Additionally, it is found that aniline can be sulfonated easily in a low acidic medium through the electrophilic attack of DBSA, leading to varied product morphology depending on the nanoparticles.

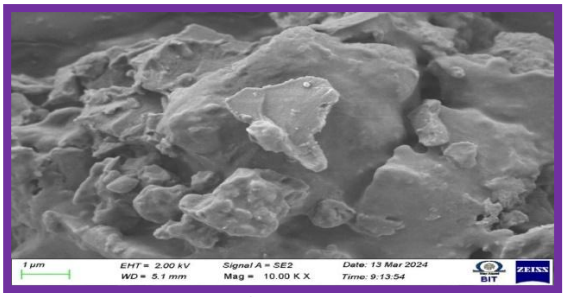

Fig.5.5 SEM morphology of Poly(ani-o-toluidine)-MnO_2-CuO nanocomposites

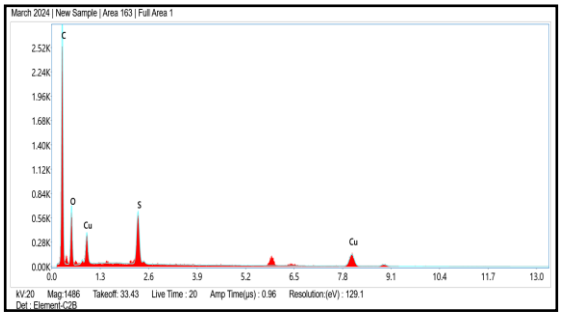

Fig.5.6 EDAX spectrum of Poly(ani-o-toluidine)-MnO_2-CuO nanocomposites

Fig 5.6 displays the EDAX analysis performed on the Poly(ani-o-toluidine)-MnO2-CuO nanocomposites to determine their atomic percentage. The quantitative analysis results indicate the presence of carbon, sulfur, manganese, copper, and oxide in the polymer composites and confirms presence CuO in the prepared sample.

The composition of the composite has been investigated through energy dispersive analysis (EDAX) conjoined with scanning electron microscopy. The elemental atomic percentages of C, S, Cu, and O present in the composite are enumerated in Table 5.5.

Table 5.5 Atomic percentage of PANI-MnO2-CuO

Element	Weight %	Atomic %	Error %	Net Int.	R	A	F
C K	75.54	83.15	10.35	780.45	0.9329	0.1430	1.0000
O K	18.27	15.10	12.58	203.13	0.9411	0.0641	1.0000
S K	2.29	0.94	4.28	279.53	0.9626	0.8560	1.0109
Cu K	3.90	0.81	6.88	109.75	0.9848	0.9970	1.1452

The scanning electron microscopy (SEM) images of all the sample pellets were taken by scanning electron microscope. Scanning electron microscopy (SEM) is used here to study the surface morphology of the samples. The particle size and surface morphology were dependent on the type and concentration of surfactant, because the surfactant was adsorbed physically to the growing polymer .Fig.5.3 shows the surface morphology of less continuous structure. The analysis of the surface morphology of the epoxy resin fractures, using SEM image (fig 5.3) finally confirmed the observation made. In modified resins are characterized by a less continuous structure, caused by lower packing of molecules in the polymer chains. It is easy to notice a less homogeneous structure (fig 5.3), which results from the presence of structures connected by interactions in the form of hydrogen bonds. The morphology of the material has been confirmed with the formation of organic and inorganic materials poly(ani;o-tol);MnO_2,CuO. This result was supported as above from the X-ray diffraction

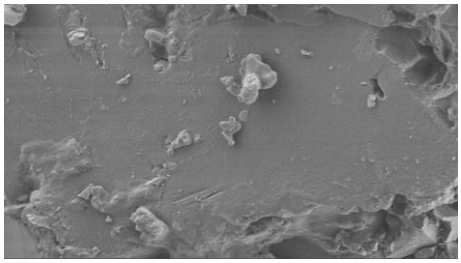

Fig 5.3(a) For SEM analysis poly(ani;o-tol);MnO_2,CuO

EDX ANALYSIS:

This fig 5.3 (b) represented by the EDX analysis of the sample **(**a)poly(ani;o-tol);MnO_2,CuO

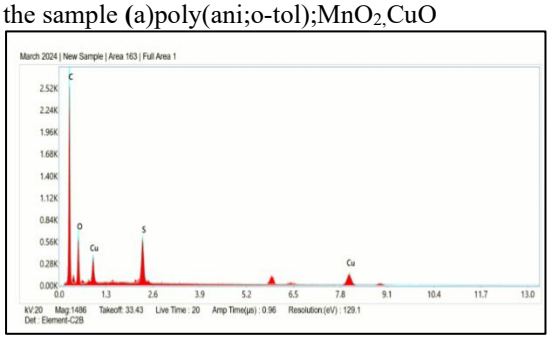

Fig 5.3(b) for EDX analysis (a)poly(ani;o-tol);MnO_2 and (b)copoly(ani;o-tol);MnO_2,CuO

SEM morphology of the Poly(ani:O-tol)-MnO2-CuO nanocomposites are shown in Fig. 5.3(a).The particle in Fig 5.3a is formed by the agglomeration of small grains of sizes smaller to 1 mm,with the laminar structure characteristic of these materials. Uniform surface with good aggregation (Fig 5.3a) of DBSA doped Poly(ani:O-tol)-MnO2-CuO is confirmed. Higher magnification (Fig 5.3b) shows the development of sponge like structure with aggregation of small uniform sized granular domains in the prepared Poly(ani:O-tol)-MnO2-CuO nanocomposites. With the addition of nanoparticles, the nanocomposites exhibits varied morphology (Fig 5.3b). Furthermore, aniline can also be sulfonated easily in low acidic medium through the electrophilic attack of DBSA. Thus, depending on the nanoparticles, the product morphology is found to be varied. Fig 5.3 (b) shows the EDAX performed to determine the atomic percentage of Poly (ani:O-tol)- MnO2-CuO nanocomposites. The quantitative analysis result indicates the presence of carbon, sulfur,Manganese, copper, and oxide in the polymer composites. Also, the result confirms the presence of CuO in the prepared sample.

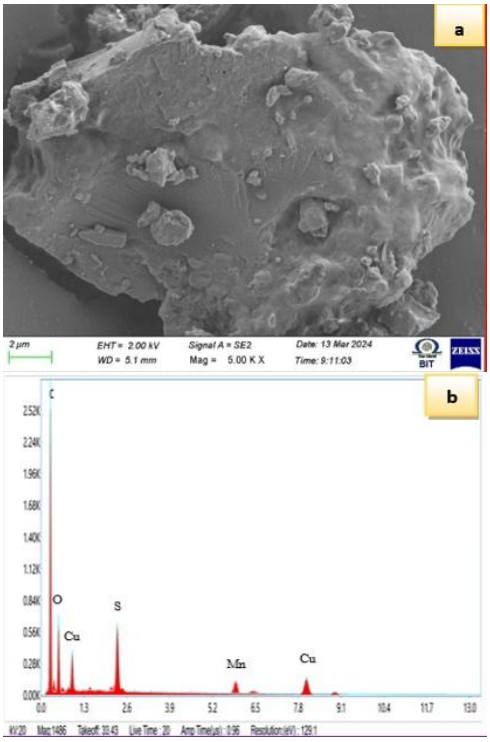

Fig. 5.3 Sem morphology and EDAX of Poly(ani:O-tol)-MnO2-CuO nanocomposites

The composition of the composite is investigated by energy dispersive analysis (EDAX) attached with scanning electron microscopy. Elemental atomic percentage of C, S, Cu and O elements presentin the composite table is listed in Table 5.2

Table 5.3 Atomic percentage of PANI-MnO2-CuO

Element	Weight %	Atomic %
C K	75.54	83.15
O K	18.27	15.10
S K	2.29	0.94
Cu K	3.90	0.81
Mn K	2.67	0.43

The scanning electron microscopy (SEM) images of all the sample pellets were taken by scanning electron microscope. Scanning electron microscopy (SEM) is used here to study the surfacemorphology of the samples. The particle size and surface morphology were dependent on the type and concentration of surfactant, because the surfactant was adsorbed physically to the growing polymer. Fig.5.1 shows the surface morphology of PANI+MnO2 + ZrO2and copolymers (PANI+ MnO2 +CdO However the dependence of the size and homogeneity of the particles only from concentration of surfactant. Adsorption of the surface active agent on the ZrO2, CdO are primarily due to the hydrophobic components in the surfactant, probably via a hydrogen bonding mechanism with the aniline N-H group [20]. The SEM images of PANI-MnO2 +CdO copolymers (Fig 5.1)shows that a gradual change from sponge like structure in to a cage like morphology having more

porous.

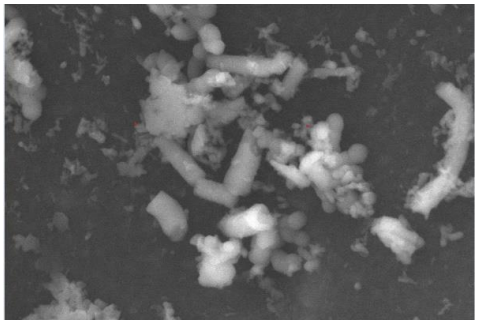

Fig 5.1 SEM analysis (a) PANI-MnO2- ZrO2, (b) Pani+ MnO2+CdO

EDAX Analysis

The chemical composition of polymer was further confirmed by EDAX analysis spectrumPani-MnO2-ZrO2 and Pani-MnO2-CdO of copolymers gave peaks for C, O, S and cd and weight percentage.

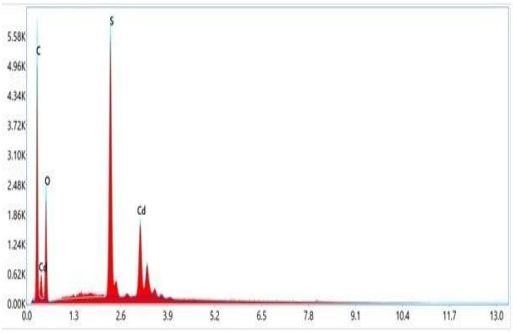

Fig 5.2 EDAX Analysis a) PANI-MnO2- ZrO2, (b) Pani+ MnO2+CdO

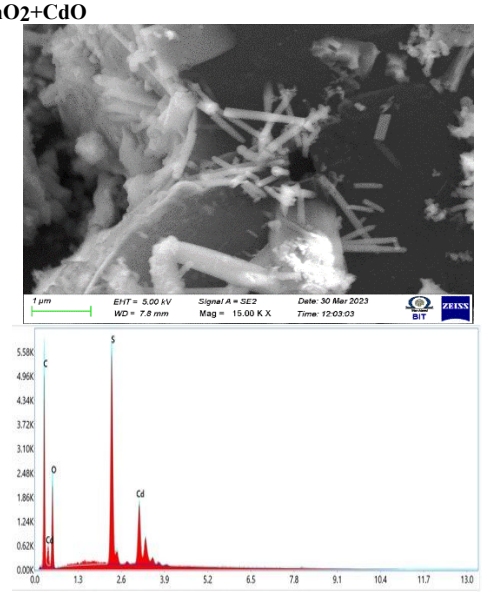

Solubility Analysis:

The solubility of the DBSA doped polymer nanocomposites (sample A and B) has been carried out in various solvents such as NMP, DMSO, ethanol and de-ionized water and the resultsare depicted in the Table 5.1. The polymer nanocomposites less soluble in water, DMSO and NMP. The increase in the solubility is due to the presence of the carboxylic acid group present in the organic molecule that increases the flexibility of the rigid polyaniline and lowering of the stiffness ofthe polymeric chains. The copolymer exhibits good solubility in ethanol without sacrificing the electrical conductivity.

Table 5.1 Solubility results for polymer nanocomposites

Sample Code	Water	Ethanol	DMSO	NMP
Poly-(ani:O-tol) + MnO2 (Sample A)	IS	S	S	S
Poly-(ani:O-tol) + MnO2 + CuO (Sample B)	IS	S	IS	IS

(IS – Insoluble, S – Soluble)

Fig 5.1 shows the graphical representation of the solutions which are dissolved in various solvents.

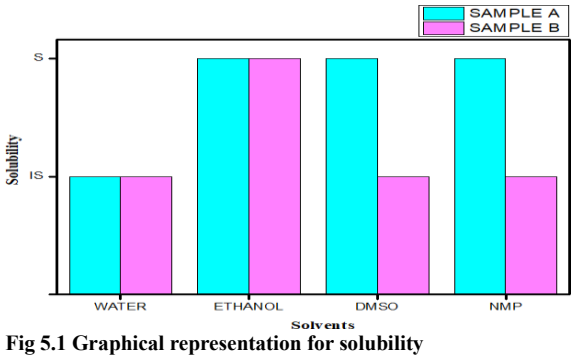

Fig 5.1 Graphical representation for solubility

The solubility of the DBSA doped pani(ZrO2 – CdO) copolymers ans silver dispersed DBSA doped pani(ZrO2 – CdO) copolymer has been carried out in various solvent such as NMP,DMSO,ethanol and water and the results are depicted in tha table 1.The copolymer and the silverdispersed copolymers are readily soluble in the polar solvents but less soluble in water and ethanol. The increase in the solubility is due to the prsence of the carboxylic acis group present in the aniline molecules that increase the flexibility of the rigid polyaniline and lowering of the stiffness of the polymeric chains .The acid group present in the aniline molecules could take part in hydrogen bonding and salvation.The copolymers exhibits good solubility without sacrificing the electrical conductivity.

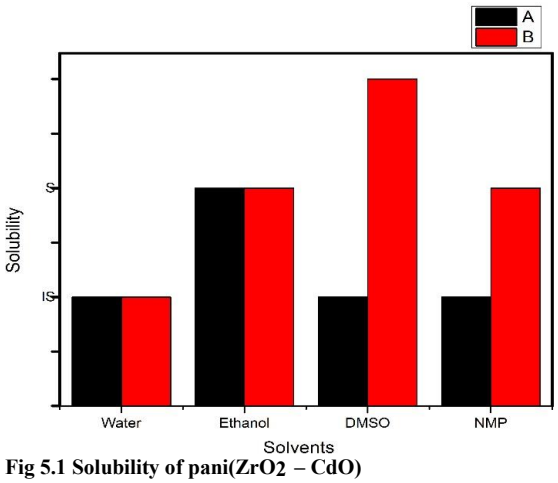

Fig 5.1 Solubility of pani(ZrO_2 – CdO)

Table 5.1 Solubility results for polymer nanocomposites

Sample code	Water	Ethanol	DMSO	NMP
Pani+MnO_2+ZrO_2	IS	S	IS	IS
Pani+ MnO_2+CdO	IS	S	PS	S

(IS – Insoluble, S – Soluble, PS – Partially soluble)

RELATIVE HUMIDITY SENSOR ANALYSIS:

Humidity sensor analysis was used to plot a graph against Relative Humidity vs Resistance.

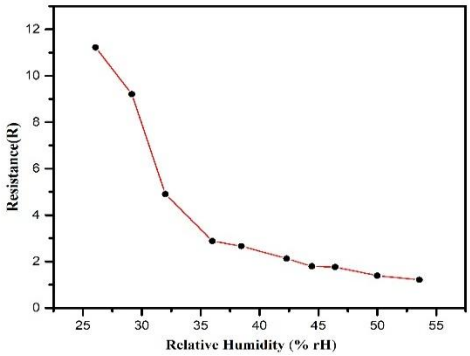

Fig.5.4. Humidity sensor analysis of Poly(ani-o-toluidine) +MnO_2+CuO

Fig 5.4 shows the relationships of capacitance and impedance with relative humidity for the Poly(ani-o-toluidine) +MnO_2+CuO sensor. It can be seen that the resistance(R) decreases with the increase in relative humidity. The table 5.4 shows the change in resistance with relative humidity(%rH).

Table.5.4. Humidity sensor analysis of Poly(ani-o-toluidine) +MnO_2+CuO

S.No	Temperature (T1)	Temperature (T2)	Relative Humidity (%RH) = Ew (T1) / Ew (T2) * 100	Resistance (R)
1	6	23	26.09	11.217
2	7	24	29.17	9.2015
3	8	25	32.00	4.9029
4	9	25	36.00	2.8835
5	10	26	38.46	2.662
6	11	26	42.31	2.1265
7	12	27	44.44	1.7929
8	13	28	46.43	1.7587
9	14	28	50.00	1.3937
10	15	28	53.57	1.2115

The change in relative humidity value are plotted against the corresponding value of resistance and the obtained humidity response curve for MnO_2-CdO hybrid composites are shown in Fig 5.5

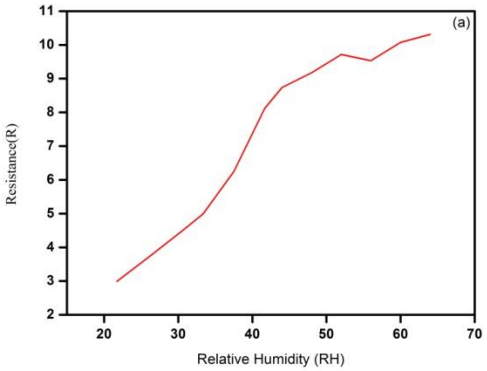

The change in relative humidity values are plotted against the corresponding values of resistance and the obtained humidity response curve for (PANI-MnO_2- ZrO_2) composite is shown fig.

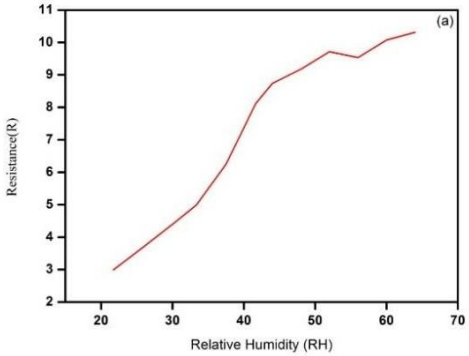

Fig 5.2 Characteristics response curve of (a) PANI-MnO2-ZrO2,

Fig5.2 (a) show a rapid resistance increase up to 35% RH, then show slight resistance variation up to 45%RH with humidity decrease. The decrease in resistance with increase humidity can be attributed to the mobile dopant ionswhich are loosely attrached to the polymer composite chains by weak Vander Walls force of attraction. At low humidity ,the

mobility of the dopant ions is restricted because the polymers chains would tendto curl up into compare coil.

$$P = RT/V-b - a/V^2$$

CONCLUSION:

REFERENCES:

1. Siqi Li, Pengfei Lin, Liupeng Zhao, Chong Wang, Deye Liu, Fangmeng Liu, Peng Sun,Xishuang Liang, Fengmin Liu, Xu Yan, Yuan Gao, Geyu Lu, "The room temperature gas sensor based on Polyaniline@flower-likeWO3nanocomposites and flexible PET substrate for NH_3detection" 2017 Published by Elsevier B.V.
2. Mahdi Karimi-Nazarabad, Elaheh K. Goharshadi, "Highly efficient photocatalytic and photoelectron catalytic activity of solar light driven WO_3/g-C_3N_4 nanocomposite" Received 16 August 2016; Received in revised form 3 November 2016, Accepted 4 November 2016,0927-0248/ © 2016 Elsevier B.V.
3. S. Sathiyanarayanan, S. Syed Azim**,** G. Venkatachari, "Preparation of polyaniline–TiO2 composite and its comparative corrosion protection performance with polyaniline" 2007 Elsevier B.V.
4. B. Manjunatha & Arjun N. Shetty & S. Kaveri & Sundar S. Mety & K. C. Anjaneya & Ramakrishna Reddy &Sangshetty Kalyane "Chemical Mediated Synthesis of Polyaniline/Tungstenoxide (PANI/WO_3) Nanocomposites and Their Antibacterial Activity Against Clinical Pathogenic Bacteria" Published online: 15 November 2019 Springer Science+Business Media, LLC, part of Springer Nature 2019.
5. D Nagesa Sastry, M Revanasiddapp, C Basavaraja, T Suresh & S C Raghavendra "DC conductivity studies of doped polyaniline tungsten oxide nanocomposites." Indian Journal of Engineering & Materials Sciences Vol. 20, October 2013, pp. 435-442.
6. Abdelghani Hsini, Yassine Naciri, Mohamed Laabd, Asmae Bouziani, J.A. Navío, F. Puga, Rabah Boukherroub, Rajae Lakhmiri, Abdallah Albourine "Development of a novel PANI@WO_3 hybrid composite and its application as a promising adsorbent for Cr (VI) ions removal" Published by :2021 Elsevier Ltd. All rights reserved.
7. Ifeanyichukwu Chinedu Amaechi1, Assumpta C. Nwanya1,2, Azubike B.C. Ekwealor1, Paul U. Asogwa, Rose U. Osuji, Malik Maaza, and Fabian I. Ezema "Electronic thermal conductivity, thermoelectric properties and supercapacitive behaviour of conjugated polymer nanocomposite (polyaniline-WO_3) thin film." Published by: 12 March 2015 – c_ EDP Sciences 2015.
8. Guijun Fan, Deliang Chen, Tao Li, Shasha Yia, Haipeng Ji, Yu Wang, Zongtao Zhang, Gang Shao, Bingbing Fan, Hailong Wang, Hongliang Xu, Hongxia Lu, Ying Zhou, Rui Zhang, Jing Sun "Enhanced room-temperature ammonia-sensing properties of polyaniline modified WO_3 nanoplates derived via ultrasonic spray process" Published by:2020 Elsevier B.V. All rights reserved.
9. Caroline B. Aquino, DaniloA. Nagaoka, MariaM. Machado, EduardoG. Cândido, Anderson G.M. da Silva, Pedro H.C. Camargo, Sergio H. Domingue. "Chemical *versus* electrochemical: What is the best synthesis method to ternary GO/WO_3NW/Pani nanocomposites to improve performance as supercapacitor." Published by:2020 Elsevier Ltd. All rights reserved.
10. Yan Wang, Xinming Wu, Wenzhi Zhang, Chunyan Luo, Jinhua Li, Qiguan Wang "3D heterostructure of graphene@Fe_3O_4@WO_3@PANI: Preparation and excellent microwave absorption performance" Published by: © 2017 Elsevier B.V. All rights reserved.
11. Prasenjit Haldar, "Achieving wide potential window and high capacitance for supercapacitors using different metal oxides (viz.: ZrO_2, WO_3 and V_2O_5) and their PANI/graphene composites with Na_2SO_4 electrolyte." Published by:2021 Elsevier Ltd. All rights reserved.
12. Ashutosh Tiwari, Shaoqin Gong. "Electrochemical Synthesis of Chitosan-co-polyaniline/WO_3 · nH_2O Composite Electrode for Amperometric Detection of NO_2 Gas." Published by: 2008 WILEY-VCH Verlag GmbH&Co. KGaA, Weinheim.
13. Narsimha Parvatikar, Shilpa Jain, Syed Khasima, M. Revansiddappa, S.V. Bhoraskar, M.V.N. Ambika Prasad, "Electrical and humidity sensing properties of polyaniline/WO_3 composites." Published by: © 2005 Elsevier B.V. All rights reserved.
14. S.B. Kulkarni, Y.H. Navale, S.T. Navale, F.J. Stadler, N.S. Ramgir, V.B. Patil"Hybrid polyaniline-WO_3 flexible sensor: A room temperature competence towards NH_3 gas."Published by: © 2019 Elsevier B.V. All rights reserved.
15. G. Jeevitha, R. Abhinayaa, D. Mangalaraj, N. Ponpandian "Tungsten oxide-graphene oxide (WO_3-GO) nanocomposite as an efficient photocatalyst, antibacterial and anticancer agent." Published by: 0022-3697/© 2018 Elsevier Ltd. All rights reserved.
16. D. Kumar "Synthesis and characterization of poly aniline-co-o-toluidine copolymer" Synthetic Metals 114 2000 369–372
17. D. Manoharan "Poly(aniline-co-o-toluidine): poly (styrene sulfonic acid) nanocolloidal self assembled multilayer thin films as a hole transport layer in organic solar cells" Materials Science in Semiconductor Processing.
18. **[18]** Manoj Kumar Ram, Elisabetta Maccioni, Claudio Nicolini "The electrochromic response of polyaniline and its copolymeric systems" Thin Solid Films 303 (1997) 27-33
19. Salma Bilal a, Anwar-ul-Haq Ali Shahb, Rudolf Holze "Raman spectroelectrochemical studies of copolymers of o-phenylenediamine and o-toluidine" Vibrational Spectroscopy 53 (2010) 279–284
20. D.D. Borole, U.R. Kapadi, P.P. Mahulikar, D.G. Hundiwale "Studies on electrochemical, optical and electrical conductivity characteristics of copolymer of polyaniline-co-poly(o-toluidine) using various organic salts" Materials Letters 57 (2003) 3629 – 3635
21. D.D. Borole, U.R. Kapadi, P.P. Mahulikar, D.G. Hundiwale "Electrochemical behaviour of polyaniline, poly(o-toluidine) and their copolymer in organic sulphonic acids" Materials Letters 58 (2004) 3816 – 3822
22. Ankita Yadav, Harish Kumar, Rahul Sharma, Rajni Kumari, Devender Singh, Osama A. Hamed "Metal oxide decorated polyaniline based multifunctional nanocomposites: An experimental and theoretical approach" Results in Engineering 18 (2023) 101161
23. Eun-Mi Kim,Chan-Keun Jung, Eun-Young Choi, Chunji Gao, Sang-Wook Kim, Suck-Hyun Lee, O-Pil Kwon "Highly conductive polyaniline copolymers with dual-functional hydrophilic dioxyethylene side chains" Polymer 52 (2011) 4451e4455
24. Soumi Dutta, Suneel Kumar Srivastava, Ashok Kumar Gupta "olypyrrole–polyaniline copolymer coated green rice husk ash as an effective adsorbent for the removal of hexavalent chromium from contaminated water" Mater. Adv., 2021,2, 2431
25. Ting Li, Xue Wang, Peng yun Liu, Bin Yang, Shen Diao, Yuan Gao "Synthesis of graphene/polyaniline copolymer for solid-state supercapacitor" Journal of Electroanalytical Chemistry
26. Eftychia Grana, Dimitrios Katsigiannopoulos, Alexander E. Karantzalis, Maria Baikousi, Apostolos Avgeropoulos "Synthesis and molecular characterization of polythiophene and polystyrene copolymers: Simultaneous preparation of diblock and miktoarm copolymers" European Polymer Journal 49 (2013) 1089–1097
27. Aida Ebrahimi, Moslem Mansour Lakouraj, Vahid Hasantabar "Synthesis and characterization of amphiphilic star copolymer of polyaniline and polyacrylic acid based on calix[4]resorcinarene as an efficient adsorbent for removal of paraquat herbicide from water" Materials Today Communications
28. Nouh Aarab, Abdelghani Hsini, Abdelilah Essekri,

Mohamed Laabd, Rajae Lakhmiri, Abdallah Albourine "Removal of an emerging pharmaceutical pollutant (metronidazole) using PPY-PANi copolymer: Kinetics, equilibrium and DFT identification of adsorption mechanism" Groundwater for Sustainable Development

29. Ashwini N. Mallya, Siddhartha Panda "DFT study of iminodiacetic acid functionalised polyaniline copolymer interaction with heavy metal ions through binding energy, stability constant and charge transfer calculations" Computational and Theoretical Chemistry 1202 (2021) 113288.
30. Pi-Guey Su, Hong-Ci Syu "Electrical and humidity-sensing properties of 1-(4-carboxylic acid phenyl)-2,5-dimethyl-1H-pyrrole doped with both KOH and K_2CO_3 salts." Published by: © 2016 Elsevier B.V. All rights reserved.